

# Chapter 9

## Reinforcing Bar Corrosion

Koichi Kobayashi, Suvash C. Paul and Gideon P.A.G. van Zijl

**Abstract** Currently, a common use for strain-hardening cement-based composites (SHCC) is as a repair material, or for retrofitting reinforced concrete (RC) structures. This is due to SHCC being expected to have high resistance to substance penetration as the cracks that are produced in SHCC are fine. Equally, in retrofitting applications such as those described in Sects. 1.5.3–1.5.5, or in applications of steel-reinforced SHCC (R/SHCC) in structures in coastal regions, the corrosion of the steel reinforcement is likely to determine both durability and structural service life. Accordingly, this chapter discusses the chloride-induced corrosion of R/SHCC. From reported experimental results, chloride profiles in cracked R/SHCC have been reported in Chap. 2. Here, the chloride contents are evaluated for correlations with observed corrosion damage in the steel bars for different cover depths in cracked R/SHCC. Steel bar damage is expressed in terms of steel mass loss, corrosion depth, and reduction in yield resistance. Finally, a corrosion model is proposed for R/SHCC, incorporating crack width, crack spacing, free chloride content, and cover depth.

**Keywords** Chloride · Crack width · Crack spacing · Corrosion · Pitting

### 9.1 Introduction

As outlined in Chap. 1, strain-hardening cement-based composites (SHCC) exhibit strain-hardening behaviour in tension, due to the formation of multiple fine cracks, upon increased deformation. The width of these cracks is relatively small, typically

---

K. Kobayashi (✉)  
Gifu University, Gifu, Japan  
e-mail: ko2ba@gifu-u.ac.jp

S.C. Paul  
Nanyang Technological University, Singapore, Singapore

G.P.A.G. van Zijl  
Stellenbosch University, Stellenbosch, South Africa

less than 0.1 mm, which is potentially beneficial for resistance to the ingress of water, water-soluble substances, and gases, therefore enabling high durability. For this reason, SHCC and steel-reinforced SHCC (R/SHCC) have been used to conduct repairs or retrofitting in corrosion-deteriorated reinforced concrete (RC) structures. The reader is referred to Sects. 1.5.3–1.5.5 for applications of R/SHCC retrofitting in RC structures exposed to chloride-induced corrosion either in coastal regions or in regions of salt-based de-icing practise. In these applications, subsequent structural life depends on the corrosion resistance of R/SHCC, despite chloride exposure and crack formation under imposed strain. Another repair strategy could be to apply SHCC as an overlay onto a RC substrate to strengthen the structural system, as well as so as to protect any reinforcing steel in the substrate from corrosion, as was alluded to in Sect. 8.6 in the previous chapter. In this chapter, the focus is on the corrosion of steel-reinforcing bars in R/SHCC.

Until now, only limited SHCC-related data have emerged from both field and laboratory experimental testing. Currently, no corrosion model exists for this new type of construction material, with the existing corrosion models for conventional RC also being open to criticism due to the fact that they sometimes either overestimate or underestimate the actual amount of corrosion occurring (Otieno et al. 2010).

Corrosion is a complex deterioration mechanism and there is no direct way of determining the actual corrosion rate, which complicates corrosion modelling and model parameter characterisation. In this chapter, non-destructive methods are used to measure the corrosion rate, and final verification is based on destructive methods to remove the bars for the evaluation of corrosion deterioration after a particular period of exposure. So far, a limited set of parameters has been studied, including the influence of cover depth, crack spacing, and exposure duration. To a lesser extent, matrix types have been studied, in the form of a low fly ash content versus high fly ash content binder, and fine sand versus coarse sand.

Two fibre types, namely polyvinyl alcohol (PVA) and high-modulus polyethylene (PE) fibres, are considered here, based on reported experimental results in the literature. Typical chloride exposures have been chosen as cyclic wetting–drying with chloride solutions in water, which are believed not to alter the electrochemical corrosion cell expected in typical field applications in coastal regions and/or in highway infrastructure subjected to de-icing salting practices. Comparative results of R/SHCC and R/mortar subjected to high electrical potential are reported, indicating the higher corrosion resistance of R/SHCC when compared to R/mortar under these particular exposure conditions.

In RC, a focus on increasing service life relies on providing good quality, low-permeable concrete and sufficient cover depth to reinforcing steel, so as to delay the point of corrosion initiation, or to increase the so-called corrosion initiation period. This remains a scenario requiring consideration in the durability design of R/SHCC, namely the eventual depassivation of reinforcing steel in uncracked R/SHCC through the gradual ingress of chloride, oxygen and water.

However, another scenario should be considered in durability design, where crack formation due to imposed strain allows the quick ingress of deleterious

substances to the surface of the steel in R/SHCC. Under these circumstances, the initiation period may be neglected, whereas the low corrosion rate in finely cracked R/SHCC is relied upon for a suitable structural service life. The low corrosion rates in cracked R/SHCC, as reported by Miyazato and Hiraishi (2005), indicate the potential of the latter strategy. In the subsequent sections of this chapter, corrosion in R/SHCC under chloride exposure is discussed. The topics of corrosion depth, corrosion area, mass loss, and the loss of yield force of steel bars are discussed and related to the crack patterns in the R/SHCC specimens. Finally, based on these parameters, corrosion modelling is also proposed for single and multiple cracks in R/SHCC specimens.

## 9.2 Chloride Ingress into Cracked SHCC

In Sect. 2.5, ingress of chloride into cracked R/SHCC was discussed. The results of several experimental series of the exposure of cracked R/SHCC specimens to chloride are presented in the section mentioned. Methods of chloride profiling are elaborated, in terms of XRF (X-ray fluorescence), as well as in terms of chemical titration. The Ingress Potential Index ( $IPI_{Cl}$ ) and the crack width value ( $CWV$ ) developed by Boshoff et al. (2016) and Wagner (2016) respectively, and which are described in Sect. 2.2, are calculated for specific experimental specimens. The correlation between the indices in question and the total chloride content in cracked SHCC specimens is shown to be reasonable for relatively short periods of exposure, but it is regarded as being less reasonable for long periods of cyclic exposure (see Fig. 2.20). The pool of data is acknowledged not only as being limited at present, but also as requiring extension in future work. Also, the  $IPI_{Cl}$  and  $CWV$  indices do not incorporate the mechanism of chloride ion transfer in non-saturated, cracked SHCC, for which further research is recommended.

Whereas a reasonable correlation has been shown between the indices and chloride content, it still remains to be seen whether there is a correlation with actual corrosion damage in R/SHCC.

## 9.3 Chloride-Induced Corrosion of Steel Bars in SHCC

Non-destructive ways of measuring corrosion rate have been proposed for RC. Such methods might offer non-destructive ways of presenting the reinforcement condition in R/SHCC. The different methods that can be used to determine the corrosion rates of specimens are influenced by various parameters, including temperature, humidity, and the presence of moisture and oxygen in the specimens concerned. Notably, a corrosion rate reading depends on the parameters and conditions prevailing at the time when the measurement is taken. Therefore, the corrosion rate value cannot be expected to remain consistent, since the aforementioned

parameters may vary from day to day, for which compensation must be made. Also, various readings over time are required so as to be able to estimate the actual state of corrosion damage. Due to corrosion, the cross-section of a steel bar reduces either uniformly, or in localised, pitting fashion, resulting in a reduction of its tensile resistance capacity. Paul and Van Zijl (2014) proposed Eq. 9.1 for estimating the uniform corrosion depth of the steel bar ( $d_c$ ) when the corrosion rate of a steel bar, over time, is known. Since mass loss and tensile resistance/force capacity loss are related to the section loss of steel bars, Eq. 9.1 allows for the estimation of its mass and resistance loss due to corrosion in cases of uniform corrosion:

$$d_c(t) = d_{c0} + \int_0^t V_{corr} dt = d_{c0} + \sum_{i=1}^{N_i} \frac{1}{2} (V_{corr} + V_{corr,i-1})(t_i - t_{i-1}) \quad (9.1)$$

with:

$d_{c0}$  the initial corrosion depth  
 $V_{corr}$  the corrosion rate (mm/year)  
 $t_i$  the period of corrosion

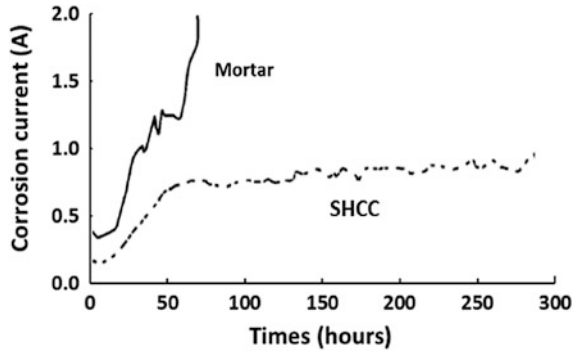
### 9.3.1 Rate of Corrosion of Steel Bars in R/SHCC

The corrosion rate in SHCC class materials has been examined by several researchers (Şahmaran et al. 2007, 2008; Kobayashi et al. 2010; Mihashi et al. 2011; Paul 2015; Jen and Ostertag 2016) over the last few years. All the authors mentioned have reported the superior performance of SHCC materials over standard repair, and other mortars, as well as over conventional concrete. However, different methodologies for corrosion measurement were used by the different researchers, and the link to the specific exposure and deterioration process has not yet been made clear in all cases.

#### 9.3.1.1 Uncracked Lollypop Specimens

Şahmaran et al. (2008) exposed SHCC and mortar lollypop-shaped specimens with centrally embedded steel bars to 5% NaCl solution, applying a potential of about 30 V to the steel bar. The steel bars had an SHCC/mortar covering of approximately 30 mm. Crack formation in the mortar and SHCC specimens, due to the corrosion of the steel bars, was monitored. After 300 h of testing, the corrosion current in the SHCC specimen was below 1 A, whereas the corrosion current was more than 1.5 A after 75 h of testing in the case of the mortar specimen (see Fig. 9.1). A single large crack of about 2 mm wide was observed to have formed in the mortar specimen parallel to the steel bar, whereas multiple fine cracks, of about

**Fig. 9.1** Observed corrosion currents in R/SHCC and R/mortar (Şahmaran et al. 2008)



0.01 mm in width, were found in the SHCC specimens after the same accelerated corrosion testing had taken place. Almost 12% mass loss of steel was observed in the mortar specimen after 75 h of the accelerated corrosion testing, whereas no, or insignificant, mass loss of the steel bar was noticed in the case of the SHCC specimen. After 300 h of accelerated testing, mass loss of 18% was found in the steel bar in the SHCC specimen. The researchers concerned concluded that, if a 0.3 mm wide crack width is considered to be a serviceability limit state for a structure, the service life of R/SHCC would be 15 times as high as that of R/mortar concrete structures.

**9.3.1.2 Cracked Specimens, w/c = 0.3, Polarisation Method**

Miyazato and Hiraishi (2013) investigated the corrosion rate in flexurally cracked high-performance fibre-reinforced cementitious composite (HPFRCC) and mortar specimens with w/c ratios of 0.3 and 0.6. Specimens were exposed to 3% NaCl solution, with penetration being allowed only through the cracked face of the specimen by means of capillary absorption, as the other faces of the specimen were sealed with epoxy resin. Such exposure was maintained for two days, followed by drying for five days, with the same cycle being followed for 28 days. Using the polarisation resistance corrosion measurement technique, for w/c of 0.3, corrosion rates of 0.082 and 0.004 mm/year were found respectively in R/mortar and R/HPFRCC specimens. The reason for the lower corrosion rate of the latter material was understandable in terms of the shallower crack depth and the smaller crack width of such specimens in comparison to those of the mortar specimens. Also, the multiple small cracks in the R/SHCC, by means of which chloride had penetrated to the level of the steel in various positions, enabled the formation of microcell corrosion, rather than the macrocell corrosion that had occurred in the R/mortar at the location of the single large crack.

### 9.3.1.3 Macrocell Versus Microcell Corrosion

In the above-mentioned research undertaken by Miyazato and Hiraishi (2013), the corrosion rates in the R/SHCC type specimens were found to be significantly (15–20 times) lower than they were in the R/mortar specimens. Insignificant corrosion was also observed in the case of steel reinforced ductile-fibre-reinforced cementitious composite (R/DFRCC) beams containing multiple cracks, compared to the amount of corrosion that was observed in cracked RC beams by Maalej et al. (2003). Significant macrocell corrosion (according to the lower anode to cathode area ratio) was found in singly cracked R/mortar in comparison to the insignificant corrosion that was found to occur in multiply cracked R/SHCC specimens, due to the formation of dominantly occurring microcell corrosion (according to the higher anode to cathode area ratio) by Miyazato and Hiraishi (2005). In terms of electrochemical corrosion processes, relatively high anode to cathode area ratios betoken a relatively high resistance of ion movement. As a result of such resistance, the corrosion damage that is due to microcell formation in steel bars tends to be relatively low. However, in contrast, in terms of macrocell corrosion, a large cathode area is paired with a small area of anode, and the ion movement from the cathode to the anode is high. The high ion movement in macrocell corrosion leads to the formation of localised pitting corrosion damage at the anode, which significantly reduces the cross-section of the steel bar. For example, it is believed that the corrosion damage in a steel bar, due to the presence of a corrosion rate of 0.5 mm/year in a relatively small anode area, is much higher than is the same corrosion rate in a larger anode area (Song and Shayan 1998).

#### 9.3.1.4 Cracked Specimens with Different Cover Depth

The corrosion rate in R/SHCC specimens with different cover depths (15, 25, and 35 mm, denoted by C15, C25, and C35) and a single reinforcing steel bar (B1) was measured by means of a Coulostatic method, as is shown in Fig. 9.2, by Paul and Van Zijl (2014). Specimens, which were stored in the laboratory at ambient temperature, were subjected to accelerated chloride exposure in the form of cyclic wetting (3 days), with chloride solution in water (3.5% NaCl), and drying (4 days). The corrosion rate reading was taken once a week. Wiggles in the corrosion rate readings are evident in Fig. 9.2, the presence of which was ascribed to sensitivity to variations in the temperature, humidity, and moisture content of the specimens. However, upon integration, according to Eq. 9.1, relatively smooth corrosion depth ( $d_c$ ) values, as shown in Fig. 9.3, were found, allowing for improved interpretation of steel bar corrosion in the various specimens tested.

Corrosion depths that were calculated in the above-mentioned way were found to be relatively high for small steel bar cover depths. In the specimens concerned, the total chloride content at the steel surface level was found, generally, to be relatively high (see Fig. 2.16). The relationship between free and total chloride

**Fig. 9.2** Corrosion rate in different cover depths of R/FS2 (fine sand) and R/CS2 (coarse sand) specimens with single steel bars (B1) (Paul and Van Zijl 2014)

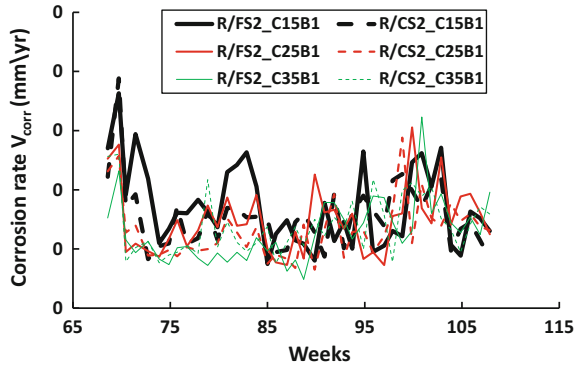
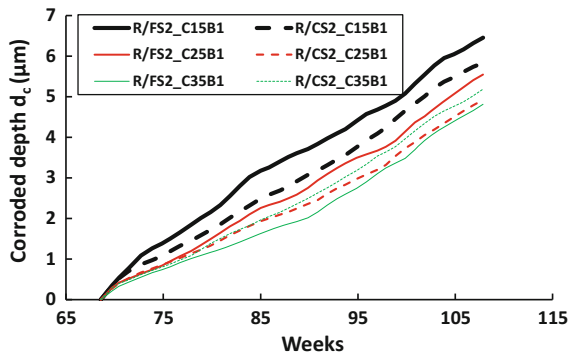


**Fig. 9.3** Estimated corrosion depths in different cover depths of R/FS2 (fine sand) and R/CS2 (coarse sand) specimens with single steel bars (B1) (Paul and Van Zijl 2014)



derived from water-soluble and acid-soluble chemical titration testing, as given in Fig. 2.18, may be relevant for the particular SHCC matrix type used.

Another advantage of SHCC, in terms of preventing rebar corrosion, is the large unit mass of the binder in its mixture. This results in a great capacity for binding/fixing chloride, whereby a relatively low amount of free chloride that damages the passive film on the rebar, is available.

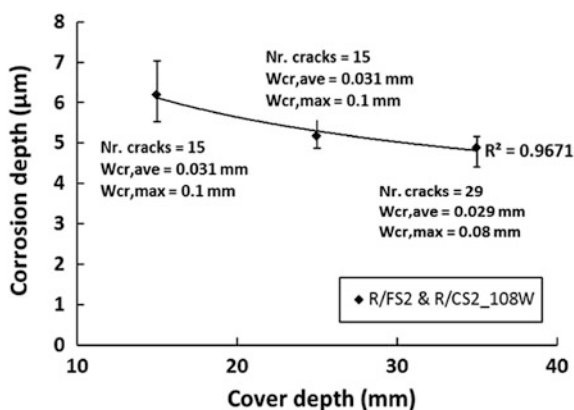
The correlation between cover depth, crack characteristics, and corrosion depth is discussed in the next section (see Figs. 9.2 and 9.3). The correlations in Sect. 9.3.2 were validated by means of actual inspection and measurement of the steel bars taken from specimens. Pitting depths, the loss of yield resistance, and the mass loss of steel bars reflect such corrosion damage (see Sect. 9.3.3).

### 9.3.2 Influence of Cover Depth, Cracks and Chloride on Corrosion in R/SHCC

Figure 9.4 shows the influence of cover depth on corrosion depth in R/SHCC specimens made from fine sand (R/FS2, with a maximum sand particle size of 0.30 mm) and coarse sand (R/CS2, with a maximum sand particle size of 1.70 mm) under conditions of chloride capillary absorption exposure for precracked specimens in the unloaded condition (Series 1, FS2), as was described in Sect. 2.5. The materials composition was reported on in Table 2.2, with such crack properties as the number of cracks, average and maximum crack widths ( $W_{cr,ave}$  and  $W_{cr,max}$ ) in a gauge length of 200 mm of a total of 500-mm-length R/SHCC specimens under conditions of flexural testing are also shown in Fig. 9.4. Corrosion depths were found to be relatively low for the comparatively high cover depth of steel bars, with an apparent threshold of between 25 and 35 mm cover depth in the particular case under discussion.

The influence of average crack width and average crack spacing on corrosion depths in the R/FS31 specimens (Series 2 by Paul (2015) in Table 2.2) is shown in Fig. 9.5. The corrosion depth was found, generally, to be relatively large for comparatively large average crack widths, and for relatively large crack spacing. The possibility that the average crack width and spacing were most likely not independent warrants further investigation. Finally, the corrosion depths versus total and free chloride contents at the surface of steel bars in the different R/SHCC specimens are shown in Fig. 9.6. Free chloride content was found to be relatively strongly correlated to the corrosion involved.

**Fig. 9.4** Relationship between  $d_c$  (Eq. 9.1) and cover depth (Paul 2015)





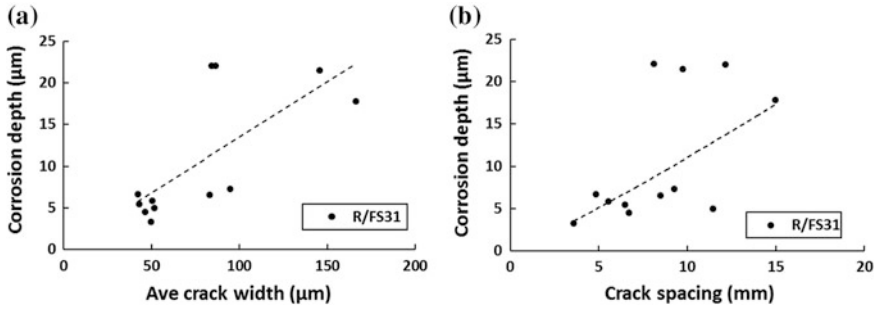
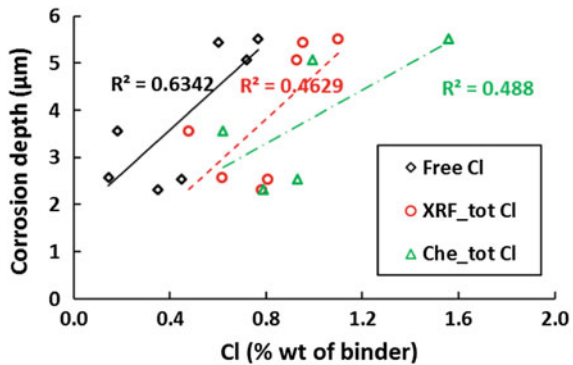


**Fig. 9.5** Influence of **a** average crack widths and **b** crack spacing on corrosion depth in R/SHCC specimens, after 57 weeks of exposure (Paul 2015; Paul and Van Zijl 2016)

**Fig. 9.6** Relationship between corrosion depth and chloride content (Paul 2015; Paul and Van Zijl 2016)



### 9.3.3 Progress of Steel Bar Corrosion Deterioration

In the case of ordinary concrete, the intrusion of water and of deleterious ions that cause deterioration is increased by the occurrence of corrosion cracking in the cover concrete, which accelerates the corrosion concerned. However, in SHCC, even if corrosion does occur, the subsequent expansion and corrosion cracking is restrained, so the rate of progress of the deterioration tends to be relatively insignificant. The current section describes corrosion damage in the steel bar.

Subsequent to the non-destructive testing of corrosion rates by Paul (2015), which has been described in Sects. 9.3.1 and 9.3.2, steel bars, on their removal from the specimens involved, were inspected for actual corrosion damage. In addition, other researchers have performed destructive testing, so as to be able to characterise the actual corrosion damage, as is reported in the following subsections.

### 9.3.3.1 Corrosion Area in Steel Bar

Kobayashi et al. (2010) used HPFRC containing three different fibre volume percentages as a surface repair coating (above steel reinforcement) as well as as a patch repair material stretching behind the steel reinforcement (see Fig. 9.7) of RC specimens. The corrosion protection performance of the repairs concerned was observed. Cracks were formed in the specimens by means of tensile testing, after which 3% NaCl solution was sprayed over the specimens for five minutes every six hours for 60 days of accelerated corrosion testing. The steel bars were subsequently removed, and the corrosion area was expressed as a percentage of the total bar surface area. To determine the corrosion area involved, the outline of each bar was traced onto a plastic sheet, with the corrosion area then being measured in relation to the discoloured area, by means of the use of a planimeter (see Fig. 9.8 for the corrosion areas). A minimum of 2% to a maximum of 10% corrosion area was

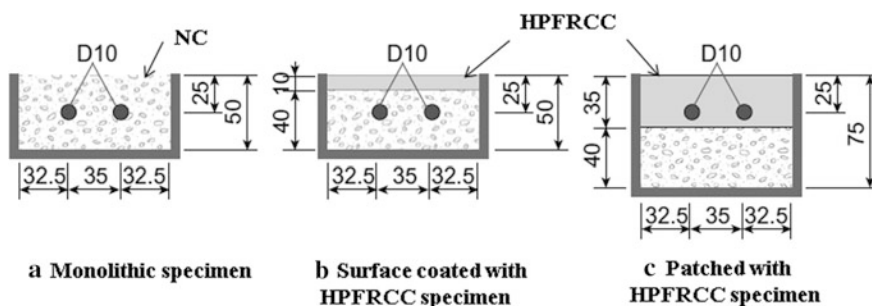


Fig. 9.7 Applied HPFRC in RC specimens (Kobayashi et al. 2010)

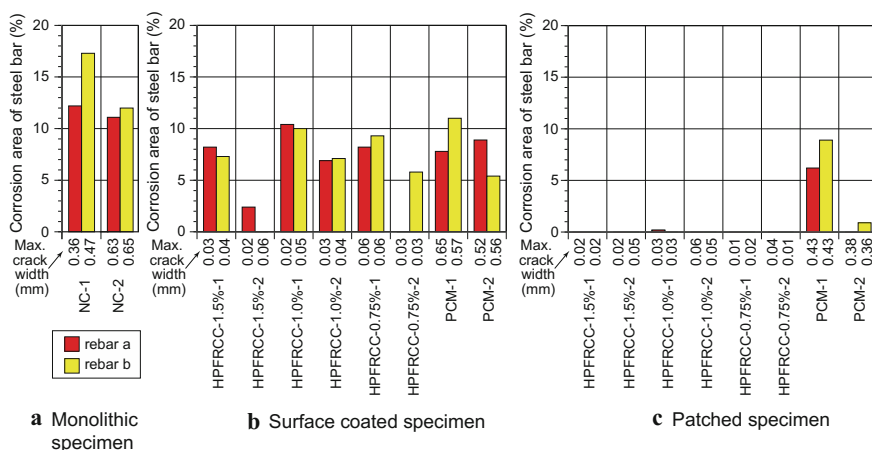


Fig. 9.8 Corrosion areas on the two steel rebars in each specimen (Kobayashi et al. 2010)

observed in all the steel bars that were present in the surface-coated specimens. However, in the patch repair specimens, significantly lower corrosion area was found in the steel bars than was found in the other specimens. The significance of the decrease concerned was ascribed to the relatively fine crack widths that formed in the HPFRCC patch repair. No significant difference was found in the performance of the HPFRCC with three different fibre contents.

Figures 9.9 and 9.10 shows the crack patterns of the R/SHCC and R/mortar specimens and corroded bars that were removed from R/SHCC and R/mortar specimens (given in Table 2.2 by Paul (2015)). Note that the mortar specimens, although having the same matrix as did the SHCC specimens, contained no fibre. Both of the bars concerned are, firstly, shown uncleaned, and then after cleaning

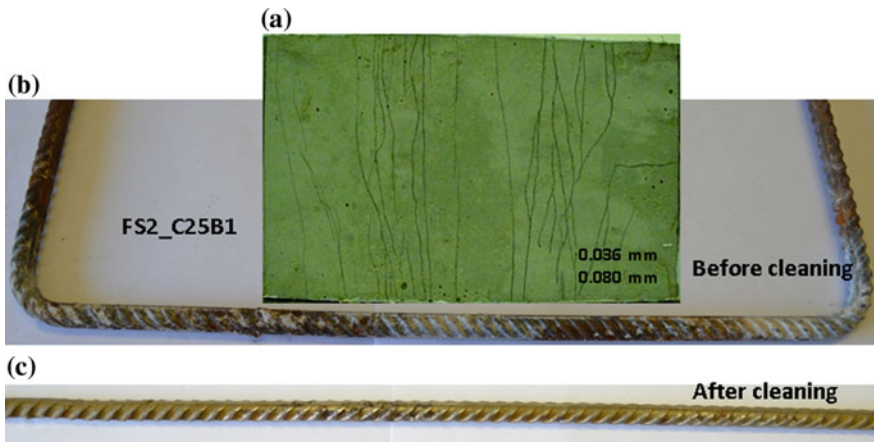


Fig. 9.9 Inspection of corrosion damage in an R/SHCC specimen (Paul 2015)

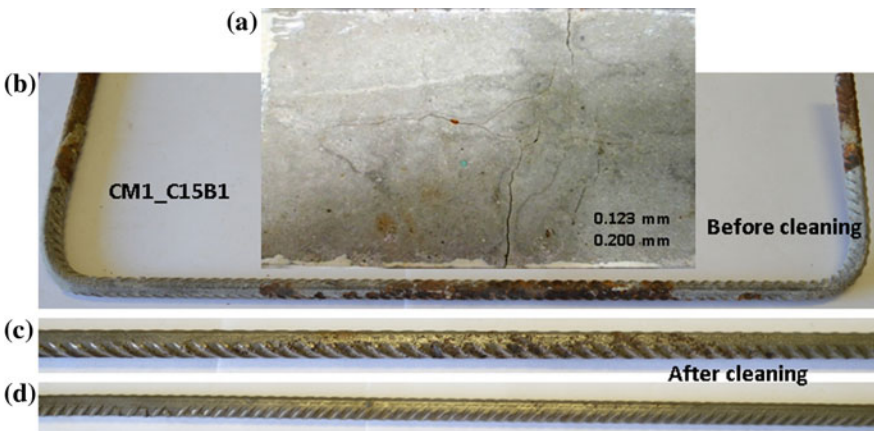
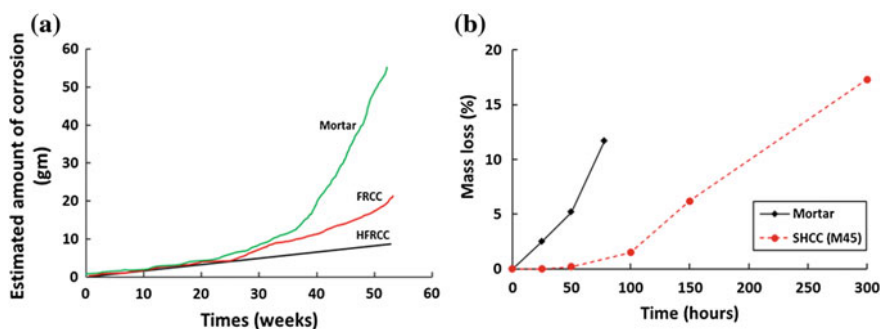


Fig. 9.10 Inspection of corrosion damage in an R/mortar specimen (Paul 2015)

with hydrochloric acid (HCl) acid. The average and maximum crack widths in the specimens are also indicated in the relevant figures. The distributed corrosion stains that were found over the entire length of the steel bar were ascribed to the presence of multiple fine cracks in the R/SHCC specimens. An increased number of corrosion activities were seen clearly outside the cracked region of the R/SHCC specimens, whereas, in the R/mortar specimens, the corrosion was more localised around the wider crack widths. The reason for the distributed corrosion in R/SHCC outside the cracked region are explained as follows: (i) The levels of deformation in the R/SHCC specimens in flexural testing were relatively high, so that delamination is likely to have occurred in the matrix and the steel surface, creating a path through which chloride could travel along the steel bar length; (ii) The parallel splitting and cracking that was also observed in some of the R/SHCC specimens enabled chloride penetration to take place parallel to the steel bars. Several cases of localised pitting corrosion areas were observed in the steel bars, especially in the cracked region of R/mortar specimens. In the R/SHCC specimens, distributed pitting was observed in the cracked region, as well as outside the cracked region. The detailed characterisation of pitting corrosion is discussed in Sect. 9.3.3.3.

### 9.3.3.2 Corrosion Mass Loss

In applying cyclic chloride exposure to uncracked hybrid fibre reinforced cementitious composites (HFRCC) and mortar beam specimens, each of which contained a single steel bar and an additional potential of 3 V to the embedded steel bar, Mihashi et al. (2011) recorded the corrosion current present for up to 52 weeks. Using Faraday's law, mass loss was calculated in the HFRCC specimens, as well as in the mortar specimens. After cyclic wetting (during which the specimens' bottom surface was submersed in 3% NaCl solution for 3.5 days) and drying (also for 3.5 days) for a year, only 10 g of mass loss was found in the HFRCC specimens, whereas, in the mortar specimens, mass loss exceeded 50 g, as is shown in



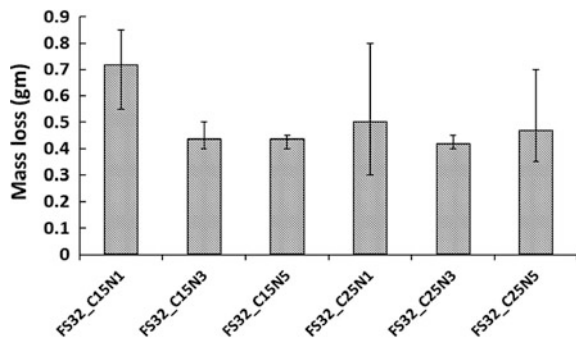
**Fig. 9.11** Mass loss versus corrosion exposure time for SHCC and mortar corrosion specimens, as reported by **a** Mihashi et al. (2011), and by **b** Şahmaran et al. (2007)

Fig. 9.11a. Also, 100% of the steel area was affected by corrosion in the mortar specimens, and a corrosion depth of about 3.1 mm was found in the original 13-mm-diameter polished rebar. In the HFRCC, only 65% of the steel area was affected by corrosion, with the depth of the corrosion being limited to 1.2 mm. The authors in question concluded that the superior crack-bridging and self-healing capacity of HFRCC may have been the reason for the relatively low mass loss in the case of the steel that was embedded in the HFRCC in comparison to the mass loss that was experienced by the steel that was embedded in the mortar. Note that the mortar and HFRCC consisted of different mix designs, unlike was the case with the testing in the case of Paul (2015).

Figure 9.11 shows the results that were achieved by Mihashi et al. (2011), and those that were achieved by Şahmaran et al. (2007), which were reported in Sect. 9.3.1, in terms of mass loss evolution over time. Both of the test series concerned were performed by subjecting the specimens involved to additional potential. In both cases, the mass loss that occurred in the reinforcement bars in the SHCC/HFRCC specimens was significantly less than was that in the reinforcement bars in ordinary, or repair-type, mortars. Furthermore, in the lollypop mortar test specimens, after corrosion cracking had taken place during the period of the test, the progression of the corrosion involved could be seen to accelerate. In contrast, in the SHCC/HFRCC test specimens, no cracks (Mihashi et al. 2011), or only fine ones (of 0.01 mm, Şahmaran et al. 2007) appeared during the test period, with no acceleration of the corrosion being observed in the case of Mihashi et al. (2011). In the case of the finely cracked lollypop SHCC specimens, only slight acceleration was observed (Şahmaran et al. 2007).

The actual mass loss of the steel bars due to the presence of the different number of cracks and crack spacing in notched R/FS32 specimens (Series 3 in Table 2.2, Paul (2015)) are shown in Fig. 9.12. The specimens involved were similar to those in Series 1 and 2, but, instead of the natural flexural crack spacing in R/SHCC, notches were sawn into the flexural face of the specimens after curing, so as to cause a single central flexural crack (in the case of specimens denoted N1), three central cracks, spaced 40 mm apart (in the case of specimens denoted N3), and five

**Fig. 9.12** Actual mass loss in the steel bars, due to corrosion in the R/FS32 specimens after 28 weeks of chloride exposure (Paul 2015), with C15 and C25 denoting 15 and 25 mm cover depth. N1, N3 and N5 denote 1, 3 and 5 notches, respectively



central cracks, spaced 20 mm apart (in the case of specimens denoted N5). Two cover depths were also considered (15 and 25 mm, which were denoted C15 and C25). Mass losses of steel bars were determined by means of measuring the weight difference before placing them in the moulds for casting, after which they were removed from the specimen, subsequent to cyclic chloride ponding exposure to the cracked face, exactly as was done in the case of Series 2. The procedure involved consisted of three days of wetting, followed by four days drying, in the loaded condition throughout, and within special steel frames, which, in the case discussed, lasted for a period of 28 weeks. Both before casting and after removal from the specimen, the bars were cleaned with HCl acid. Mass loss in the single-notch specimens was found to be higher than it was in the case of the other specimens. The heightened mass loss can be explained in terms of the increased corrosion rate in the relatively small anode area of the N1 specimens, which caused the heightening of loss in comparison to the lowered corrosion rate in the relatively large anode area specimens of N3 and N5. In R/FS32 specimens with a cover depth of 15 mm, the average mass loss in N1 specimens was 60 and 67% higher than it was in the specimens with three and five notches that were spaced 40 and 20 mm apart, respectively.

### 9.3.3.3 Pitting Corrosion Depth

Consequences of corrosion in terms of pitting depth and pitting area were also observed by Paul (2015) in R/SHCC specimens. The presence of chloride in concrete which absorbs water and retains moisture in the pores, results in an increase in the electrical conductivity in concrete. Relatively high conductivity of concrete contributes to the separation of anode and cathodes, as the ions concerned

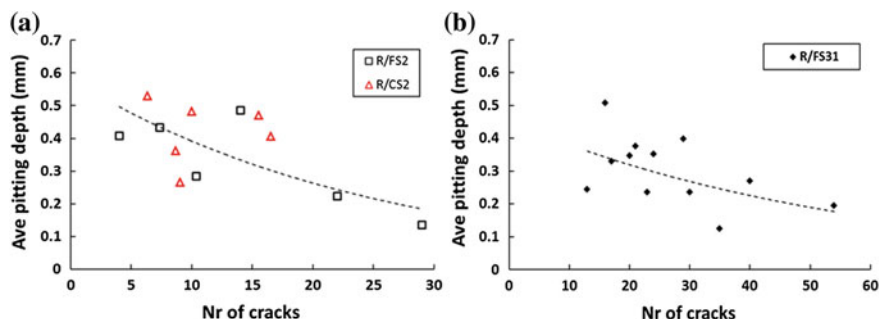


**Fig. 9.13** Pitting depth with different numbers of cracks in the 200-mm-long exposed length of R/SHCC specimens of **a** Series 1, and **b** Series 2 in Table 2.2 (Paul 2015)

can move through the water-lined pores. Due to these ions, pitting can occur in the steel bar, which can significantly reduce the steel capacity.

The corrosion pitting depths in the individual steel bars were found to be relatively low for an increased number of cracks within the exposed length of 200 mm in the R/SHCC specimens, as is shown in Fig. 9.13. The phenomenon can be explained by the fact that an increased number of cracks in the specimen over a given length naturally produces comparatively fine average crack spacing, leading to relatively small cathodic areas in comparison to the anodic area in the corrosion cell. Accordingly, comparatively few  $\text{OH}^-$  ions become available from the relatively small cathode to react with the  $\text{Fe}^+$  in the anode. In such case, the corrosion that is distributed over the lengths of steel bars is expected to have distributed pitting (see Fig. 9.9), rather than consisting of concentrated corrosion (see Fig. 9.10). Again, crack spacing and crack width are acknowledged as being somehow related, which warrants further investigation.

The correlation between the total crack width (being the sum of all crack widths in the 200-mm-long exposed surface) and the average crack spacing with the pitting corrosion depths was also studied. For total crack widths below 1 mm (in the gauge length of 200 mm of specimens tested in the current series), a trend of reduced pitting depths with increased total crack width is seen in Fig. 9.14a for Series 1 specimens, which were tested in the unloaded condition. For Series 2, which were tested in the loaded condition, relatively large total crack widths (>1 mm) occurred, with, for the present series of specimens, the trend not being as significant (see Fig. 9.14b). The trend of reduced pitting depths, with increased total crack width, may be ascribed to microcell corrosion in the steel bar, due to the presence of a relatively high number of cracks being associated with a comparatively high total crack width (see Fig. 9.15). However, the relatively high number of cracks is typically also often associated with the presence of an increased number of cracks of comparatively fine width in SHCC that is precracked by being bent to the same deflection. Thus, an increase in both the closeness of the crack spacing, and in the fineness of the crack width may have led to distributed corrosion.

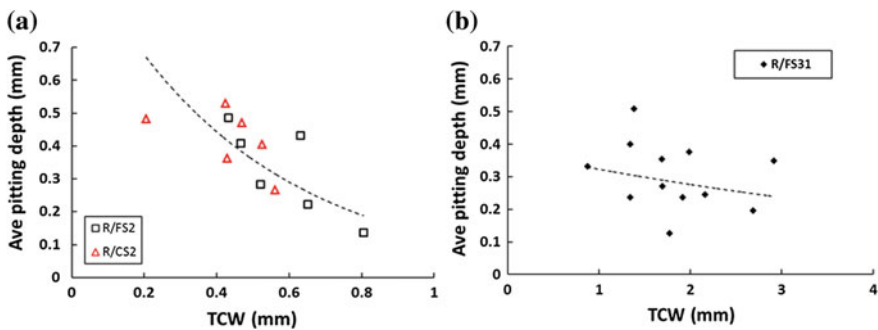


**Fig. 9.14** Average pitting depth versus total crack widths (TCWs) in R/SHCC specimens of **a** Series 1, and **b** Series 2, in Table 2.2 (Paul 2015)



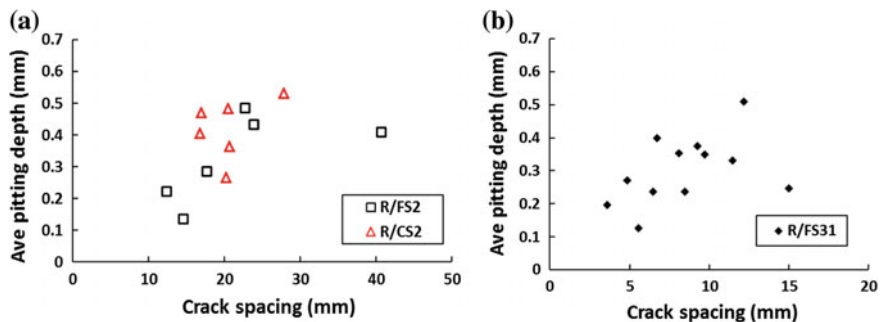


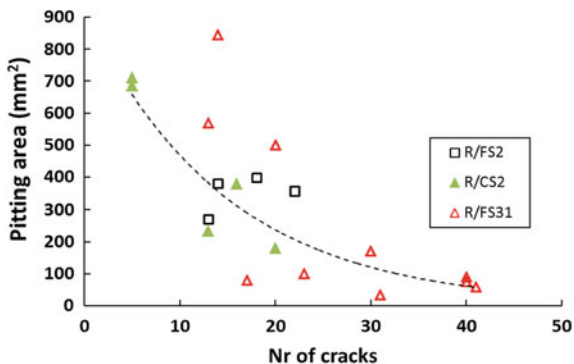
Fig. 9.15 Average pitting depth versus crack spacing in R/SHCC specimens of a Series 1, and b Series 2, in Table 2.2 (Paul 2015)

### 9.3.3.4 Localised Versus Distributed Corrosion Damage

Typically, in the steel bars studied, more severe pitting depths have been found due to macrocell corrosion than due to microcell corrosion (Broomfield 2007). The postulation was also verified by means of measuring and adding up the total pitting area in the steel bars, as is shown in Fig. 9.16 for both Series 1 and 2 in Table 2.2. The actions in question were performed after cleaning each steel bar with HCl, and then carefully marking each visible pitting area with appropriate simple surface geometrical shapes (circular, rectangular, and trapezoidal). A Vernier scale was then used to measure the marked areas accurately, so as to be able to calculate the total pitting area on the surface of each steel bar. From Fig. 9.16, it is apparent that a relatively large number of cracks in the specimens caused the lowering of the overall pitting area.

The influence of total crack widths on the steel-pitting diameter at the crack locations of the corrosion steel bars in RC was also examined by Mohammed et al. (2001). After corrosion testing had taken place, the RC specimen was broken, and the pitting diameter in the corroded steel bars was measured by means of a

Fig. 9.16 Pitting area in steel, due to the different number of cracks in the R/SHCC specimens (Paul 2015)





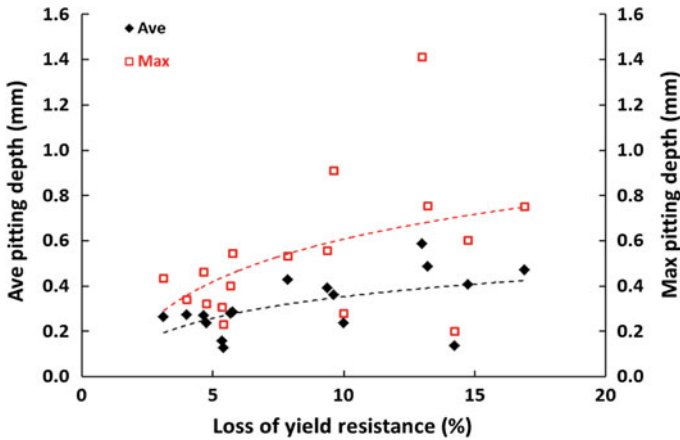


Fig. 9.17 Measured pitting depth versus the rebar loss of yield resistance (Paul 2015)

microscope, at the location of the known crack widths. A trend of decreased pitting diameters was found in the steel bars for relatively large total crack widths. Therefore, in terms of the corrosion damage of steel bars, the number of cracks, of total crack widths, and of crack spacing can be seen to be related.

Figure 9.17 shows a relationship between pitting depths and corrosion-induced loss of tensile yield resistance. An upward trend was found in the loss of yield resistance with increased pitting depth. Of importance in rebar resistance is the reduction in its cross-sectional area, which is clearly not represented by means of the pitting depth only, in the light of the rather poor correlations shown in Fig. 9.17. More accurate representation of the loss of the cross-sectional area is required to improve the correlation and estimation of corrosion damage to steel reinforcement, which is the subject of further research.

### 9.3.4 Crack Indices and Corrosion Damage

In Sect. 2.2, the  $IPI_{Cl}$  and  $CWV$  indices that were derived were subsequently applied to actual observed and experimentally obtained crack patterns and chloride profiles in Sect. 2.5.3. A reasonable correlation between the indices and the chloride content at the steel bar depth in cracked R/SHCC specimens exposed to a limited number of chloride wetting and drying cycles was shown in Fig. 2.21. However, the actual corrosion, in terms of average or maximum pitting corrosion depths, is not correlated with the indices, as is shown in Fig. 9.18 for maximum pitting depths. The above finding is to have been expected, as pitting corrosion was found to be uncorrelated to average or maximum crack widths in chloride-exposed specimens by Paul (2015), whereas the  $CWV$  is strongly correlated with average crack width, and the  $CWV_{WP}$  with maximum crack width, as is shown in Fig. 9.19.

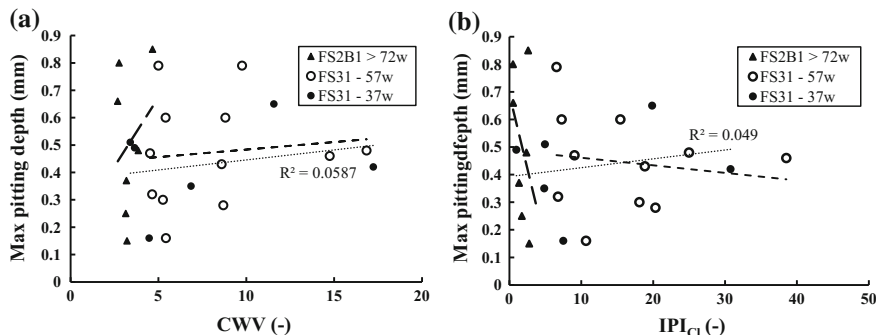


**Fig. 9.18** Maximum pitting depth observed in corroded bars by Paul (2015), in Series 1 and 2 specimens (Table 2.2), showing no correlation with **a** CWV index, and with **b**  $IPI_{Cl}$

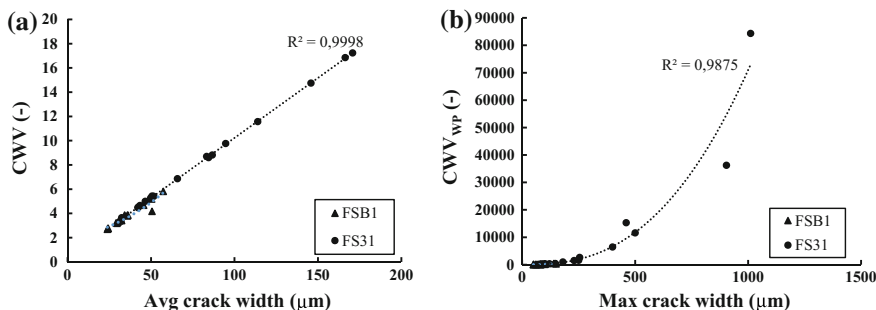


**Fig. 9.19** Correlation between **a** the CWV and the average crack width, and between **b** the  $CWV_{WP}$  and the maximum crack width, for Series 1 and 2 in Table 2.2 (Paul 2015)

### 9.3.5 Splitting Corrosion Cracking

Grubb et al. (2007) performed chloride-induced corrosion experiments on lollypop specimens, which, in the present case, were 75-mm-diameter cylindrical specimens of a length of 150 mm, with a concentrically embedded steel bar of a diameter of 9.52 mm. Two water-to-cement ratio cement-based matrices (with a w/c of 0.4 and 0.55) were used. For each w/c ratio, a set of fibre-reinforced mortar specimens was prepared containing 4.5% by volume of steel microfibres. As control, a mortar mix was prepared for each w/c ratio. At the age of 28 days, all the specimens were exposed to a 3.5% sodium chloride, aerated aqueous solution, firstly for one day standing only up to 38 mm in the solution, after which the 150-mm-high lollypop specimens were fully submerged in the solution. Acid soluble chloride content tests, giving the total chloride content, were performed on half of the specimens after 22 weeks of submergence, showing that the fibre-reinforced specimens had higher total chloride, both in their surface regions and internally, than did the control

mortar specimens for both w/c ratios. However, electrochemical testing during the 22-week submergence in NaCl solution resulted in significantly higher corrosion current densities ( $i_{corr}$ ) for the control mortar specimens than for the fibre-reinforced ones. The authors postulate that the presence of microfibrils close to the reinforcing bar served to control the splitting cracks arising from corrosion-product-induced swelling. Accordingly, the cracks concerned were eventually filled with corrosion products, which prevented further ingress of deleterious materials to the steel surface, keeping the corrosion rate low.

Jen and Ostertag (2016) performed chloride aqueous solution (3.5%) ponding on steel-reinforced beams of hybrid fibre-reinforced concrete (R/HyFRC), as well as on reinforced concrete (RC) control beams. The matrices of the control and HyFRC specimens contained the exact same amount of water, cement and fly ash content, with w/c = 0.6 and w/b = 0.45. In the HyFRC specimens, 0.2 vol% PVA fibres ( $L_f = 8$  mm,  $d_f = 0.04$  mm), together with 1.3 vol% hooked-end steel fibres ( $L_f = 30$  mm,  $d_f = 0.55$  mm) replaced some of the fine and coarse aggregate in the control specimen mixes. The cover-to-steel bar surface was 25 mm for both beam types. The small R/HyFRC and RC beams, with a cross-section of  $152 \times 152$  mm, and 610 mm long, were subjected to the same flexural load, leading to one or two wide (0.2–0.3 mm) transverse cracks, and to a longitudinal splitting crack 130–250 mm long in the RC beams, but no visible cracks in the R/HyFRC beams. After roughly two years, during which continuous ponding was maintained in the first year, and while the solution was allowed to evaporate in the second year, electrochemical measurements showed the presence of significantly higher corrosion currents in the reference RC beams ( $i_{corr} = 2.80$ , and  $6.05 \mu\text{A}/\text{cm}^2$ ) than in the R/HyFRC beams ( $i_{corr} = 0.4$ , and  $0.42 \mu\text{A}/\text{cm}^2$ ). Visibly increased crack widths in the RC beams, as well as significantly higher steel mass loss in the reinforcing bars of 8 and 12 g respectively for the bars in the RC specimens, compared with 2 and 4 g respectively for the bars in the two R/HyFRC beams, confirmed the presence of higher corrosion rates in the RC control beams. As postulated by Grubb et al. (2007), Jen and Ostertag (2016) suggest that corrosion splitting crack control by the fibres involved led to the reduced corrosion rates concerned.

In the R/HyFRC beam specimens of Jen and Ostertag (2016), the corrosion of steel fibres was noted in the part of the sample that was directly adjacent to the pond of NaCl aqueous solution. Mihashi et al. (2011) also observed dispersed corrosion stains on their hybrid fibre-reinforced ( $V_f = 1.5\%$  steel, together with 1.5% PE fibres) HFRCC beam specimens, in which they found significantly lower steel bar corrosion than they did in the R/mortar and R/FRCC (strain-softening) specimens containing only 1.5% PE fibres (see Fig. 9.11a). They postulate that the low corrosion rate observed in the steel-reinforcing bars embedded in HFRCC was caused by two mechanisms, namely crack width control by the fibre bridging, as well as the mechanism of steel fibres acting as sacrificial anodes.

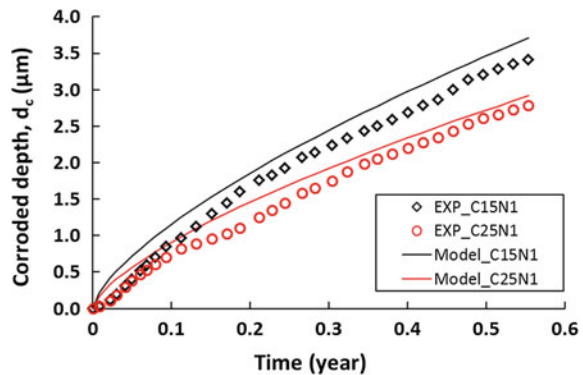
## 9.4 Towards Corrosion Modelling in R/SHCC

Long-term experimental and field data are required for the development of reliable models. Until now, the data on SHCC has been limited in both field and laboratory experimental testing. As yet, no corrosion model exists for the new type of material concerned, with the existing corrosion models for NC also being criticised by researchers, as designers sometimes either overestimate, or underestimate, the amount of corrosion occurring in steel bars (Otieno et al. 2010). The highly complex nature of corrosion has resulted in there being no direct way of determining the actual corrosion rate. As a result, there are always some differences between the experimental findings and the actual corrosion that occurs in a structure. The present section describes a corrosion model developed by Paul (2015) for exploring single and multiple cracks in R/SHCC specimens.

### 9.4.1 Empirical Corrosion Modelling of R/SHCC

A corrosion model was proposed from the results that were obtained in for R/SHCC specimens. From the corrosion testing of R/SHCC, different correlations were observed between the corrosion, the cracks, the cover depth, and the chloride content. Based on the correlations, empirical Eqs. 9.2 and 9.3 were developed to predict the corrosion depths in the steel bars, due to the chloride-induced corrosion that was found to have occurred in the R/SHCC. Whereas Eq. 9.2 is valid for a single crack, Eq. 9.3 is valid for multiple cracks in the R/SHCC specimen. In addition, the corrosion rate that was measured by Paul (2015) was based on application of the coulometric method, so that the equations in question may require adjustment before use for another corrosion rate measurement method. Figure 9.20 shows the experimental and model data for single-crack specimens with 15 and 25 mm cover depths. The multiple cracks, and the influence of crack spacing, that were also considered in the modelling of R/SHCC specimens are shown in

**Fig. 9.20** Corrosion modelling using Eq. 9.2 of cracked R/SHCC specimens with a single crack (Paul and Van Zijl 2016)



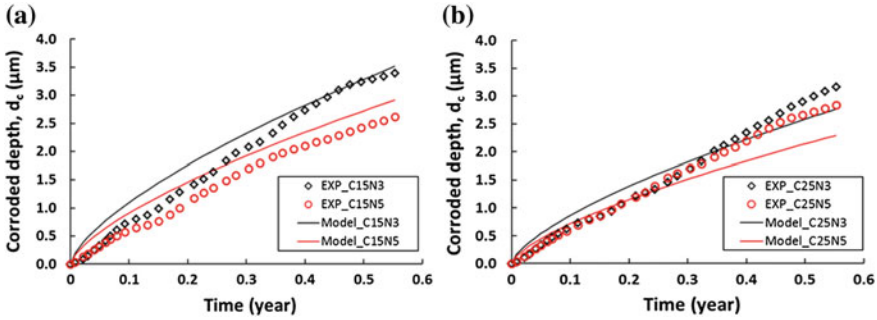


**Fig. 9.21** Corrosion modelling using Eq. 9.3 of cracked R/SHCC specimens with multiple cracks (Paul and Van Zijl 2016)

Fig. 9.21a, b. As noted, the corrosion depth models are based on the experimental corrosion rate that was obtained from the Coulostatic method, and on the estimated corrosion depths that were calculated by means of integrating the corrosion rate over time (as in Eq. 9.1). However, there are several ways of determining the corrosion rate that occurs in a steel bar. Therefore, for different corrosion methods, the models may require calibration. Also, the influence of temperature, relative humidity (RH), amount of oxygen, and moisture content in the R/SHCC specimen were not considered in the modelling. Therefore, when the aforementioned parameters are known in the SHCC, the current modelling also requires improvement.

For single-crack specimens:

$$d_c = \frac{\delta_T \delta_{RH} W_{cr,ave} t^{2t} Cl_{free}^{z_{cl}}}{C^{z_c}} \tag{9.2}$$

For multiple-crack specimens:

$$d_c = \frac{0.35 \delta_T \delta_{RH} W_{cr,ave} t^{2t} Cl_{free}^{z_{cl}} S_{cr}^{z_s}}{C^{z_c}} \tag{9.3}$$

with:

- $d_c$  the corroded depth ( $\mu\text{m}$ )
- $t$  the corrosion time (year)
- $W_{cr,ave}$  the average crack width in the specimen ( $\mu\text{m}$ )
- $Cl_{free}$  the percentage of free chloride at the steel surface level (i.e. the % wt of the binder)
- $S_{cr}$  the average crack spacing (in mm) in the specimen
- $C$  the cover depth of the steel bar

The factors that depend on the temperature and on the relative humidity (RH) at the steel-bar level are  $\delta_T$  and  $\delta_{RH}$ . At the specimen surface temperature of  $21 \pm 2 \text{ }^\circ\text{C}$ ,

the  $\delta_T$  can be considered to be 1. Similarly, for  $55 \pm 5\%$  RH,  $\delta_{RH}$  can be considered to be 1. The factors that depend on the ratio of wetting and drying periods, on the types of binder, on the range of maximum crack spacing, and on the quality of cover concrete (i.e. the microstructure and the tensile strength of concrete) are  $\alpha_r$ ,  $\alpha_{cl}$ ,  $\alpha_S$  and  $\alpha_C$ . In the current research work, the values of  $\alpha_r$ ,  $\alpha_{cl}$ ,  $\alpha_S$  and  $\alpha_C$  were considered to be 0.68, 0.5, 0.27, and 0.3, respectively. In terms of the values concerned, Fig. 9.20 shows reasonable agreement between Eq. 9.2 and the experimental data for single-crack (notched) FS32 specimens, whereas in Fig. 9.21a, b, Eq. 9.3 is shown to be in reasonable agreement with the corroded depths in the multiply cracked R/FS32 specimens. However, the values may need to be recalibrated for other material types, exposure conditions, ages, and different corrosion rate measurement techniques. In both Figs. 9.20 and 9.21, the data points represent Coulostatic corrosion rate measurements and the application of Eq. 9.1.

#### **9.4.2 Durability Design Approaches for Chloride-Induced Corrosion in R/SHCC**

At the current state of research into corrosion, the report on the corrosion rate of steel bars inside concrete is incomplete, and, in some cases, it is also contradictory. The pool of research results is limited, and no validation has been done by way of the actual field corrosion of an R/SHCC structure. In the present instance, experimental observations of the chloride-induced steel bar corrosion rates and the damage in R/SHCC are used as a basis for guidelines of the responsibilities of both the researcher and the durability designer:

- For the particular R/SHCC, the parameter values involved in the corrosion process require determining, including: (i) the crack width distribution; (ii) the crack spacing; (iii) the cover depth that may influence the crack width and spacing and the time taken for the oxygen, the free chloride, and the water to reach the steel-initiating corrosion and to enhance the corrosion rate; and (iv) the link between crack patterns and free chloride content at the level of the steel bar in the expected chloride exposure conditions.
- In laboratory experiments, and in the conditioned assessment of existing structures or structural elements, the corrosion rate requires estimating by means of such measuring techniques as the polarisation method, the Galvano static method, or the Coulostatic method.
- To improve the reliability of durability design in chloride exposure conditions, an increased data pool is required of non-destructive corrosion rate measurements, correlated with actual corrosion damage, such as pitting depth/area, mass loss, localisation of corrosion damage as a function of crack pattern, and loss in rebar resistance.

- The limit states of such parameters and the amount of damage that can be incurred before R/SHCC structures need repair or demolition require determination.

At the time of publication, no data on carbonation-induced corrosion in R/SHCC is yet available, which should be considered a worthy subject for further research.

## 9.5 Conclusions

This chapter has discussed the chloride-induced corrosion of reinforcement in SHCC, in particular when cracking occurs in the SHCC. Carbonation-induced corrosion in R/SHCC remains a research need.

In corrosion testing, greater estimated corrosion depth and actual measured and pitting depth in the steel were found in the specimens with a cover depth of 15 mm. A smaller difference was observed between specimens with 25 and 35 mm cover depths, suggesting a threshold cover thickness for specimens of this matrix type.

The average corrosion pitting depths and pitting areas in the steel bars are generally lower for R/SHCC specimens with smaller crack spacing. A reasonable correlation was found between the average pitting depths and the loss of yield force capacity of the steel bars, although localisation and cross-section reduction warrant further investigation.

The amount of free chloride content at the level of the steel bar surface appears to be better correlated to the actual corrosion damage than is the total chloride content. The experimental results of chloride-induced corrosion reported in this chapter can be represented by power functions incorporating average crack width, crack spacing, free chloride content at the steel surface, and time of exposure. Crack pattern indices developed in Chap. 2 appear to be uncorrelated to pitting depth, despite their reasonable correlation with chloride content at shorter exposure duration found in Chap. 2. It appears that crack spacing may dominate corrosion rate in cracked R/SHCC, due to the slow corrosion in the microcell chemo-electrical corrosion process.

## References

- Boshoff, W.P., Altmann, F., Adendorff, C.J., Mechtcherine, V. (2016). A new approach for modelling the ingress of deleterious materials in cracked strain hardening cement-based composites. *Materials and Structures* 49(6):2285-2295.
- Broomfield J.P. (2007). *Corrosion of steel in concrete understanding, investigating and repair*. 2nd edition, Taylor & Francis, Milton Park.
- Grubb, J.A., Blunt, J., Ostertag, C.P., Devine, T. (2007). Effect of steel microfiber on corrosion of steel reinforcing bars. *Cement and Concrete Research* 37(7):1115-1126.

- Jen, G., Ostertag, C.P. (2016). Experimental observations of self-consolidated hybrid fiber reinforced concrete (SC-HyFRC) on corrosion damage reduction. *Construction and Building Materials* 105:262-268.
- Kobayashi, K., Iizuka, T., Kurachi, H., Rokugo, K. (2010). Corrosion protection performance of high performance fibre reinforced cement composites as a repair material. *Cement and Concrete Composites* 32:411-420.
- Maalej, M., Ahmed, S.F.U., Paramasivam, P. (2003). Corrosion durability and structural response of functionally-graded concrete beams. *Journal of Advanced Concrete Technology* 1 (3):307-316.
- Mihashi, H., Ahmed, S.F.U., Kobayakawa, A. (2011). Corrosion of reinforcing steel in fibre reinforced cementitious composites. *Journal of Advantage Concrete Technology* 9(2):159-167.
- Miyazato, S., Hiraishi, Y. (2005). Transport properties and steel corrosion in ductile fibre reinforced composites. *Proceedings of 11th International Conference on Fracture (ICF11)*, 20-25 March 2005, Torino, Italy, Politecnico di Torino, Torino, CD-ROM.
- Miyazato, S., Hiraishi, Y. (2013). Durability against steel corrosion of HPFRCC with bending cracks. *Journal of Advantage Concrete Technology* 11:135-143.
- Mohammed, T.U., Otsuki, N., Hisada, M., Shibata, T. (2001). Effect of crack width and bar types on corrosion of steel in concrete. *Journal of Materials in Civil Engineering* 13:194-201.
- Otieno, M.B., Alexander, M.G., Beushausen, H.D. (2010). Corrosion in cracked and un-cracked concrete influence of crack width, concrete quality and crack reopening. *Magazine of Concrete Research* 62(6):393-404.
- Paul, S.C., Van Zijl, G.P.A.G. (2014). Crack formation and chloride induced corrosion in reinforced strain hardening cement-based composite (R/SHCC). *Journal of Advanced Concrete Technology* 12:340-351.
- Paul, S.C. (2015). The role of cracks and chloride in corrosion of reinforced strain hardening cement-based composite (R/SHCC). PhD thesis, Stellenbosch University, South Africa.
- Paul, S.C., Van Zijl, G.P.A.G. (2016). Chloride-induced corrosion modelling of cracked reinforced SHCC. *Archives of Civil and Mechanical Engineering* 16:734-742.
- Şahmaran, M., Li, M., Li, V.C. (2007). Transport properties of engineered cementitious composite under chloride exposure. *ACI Materials Journal* 104(6):243-250.
- Şahmaran, M., Li, V.C., Andrade, C. (2008). Corrosion resistance performance of steel reinforced engineered cementitious composite beams. *ACI Materials Journal* 105(3):604-611.
- Song, G., Shayan, A. (1998). Corrosion of steel in concrete: causes, detection and prediction. A state-of-art-review, ARRB Transport Research Ltd, Review Report 4.
- Wagner, C. (2016). Dauerhaftigkeitsrelevante Eigenschaften von dehnungsverfestigenden zementgebundenen Reparaturschichten auf gerissenen Betonuntergründen (Durability-related properties of strain-hardening cement-based repair layers on cracked concrete substrates). Doctoral thesis, Technische Universität Dresden, Germany.